JACS
JOURNAL OF THE AMERICAN CHEMICAL SOCIETY
Article
pubs.acs.org/JACS

Mechanistic Insight into the Formation of Cationic Naked Nanocrystals Generated under Equilibrium Control

Sean E. Doris,[†,‡] Jared J. Lynch,[†] Changyi Li,[†,§] Andrew W. Wills,[†] Jeffrey J. Urban,[†] and Brett A. Helms*[,†]

[†]The Molecular Foundry, Lawrence Berkeley National Laboratory, One Cyclotron Road, Berkeley, California 94720, United States
[‡]Department of Chemistry and [§]Department of Chemical and Biomolecular Engineering, University of California, Berkeley, California 94720, United States

Supporting Information

ABSTRACT: Cationic naked nanocrystals (NCs) are useful building units for assembling hierarchical mesostructured materials. Until now, their preparation required strongly electrophilic reagents that irreversibly sever bonds between native organic ligands and the NC surface. Colloidal instabilities can occur during ligand stripping if exposed metal cations desorb from the surface. We hypothesized that cation desorption could be avoided were we able to stabilize the surface during ligand stripping via ion pairing. We were successful in this regard by carrying out ligand stripping under equilibrium control with Lewis acid−base adducts of BF_3. To better understand the microscopic processes involved, we studied the reaction pathway in detail using in situ NMR experiments and electrospray ionization mass spectrometry. As predicted, we found that cationic NC surfaces are transiently stabilized post-stripping by physisorbed anionic species that arise from the reaction of BF_3 with native ligands. This stabilization allows polar dispersants to reach the NC surface before cation desorption can occur. The mechanistic insights gained in this work provide a much-needed framework for understanding the interplay between NC surface chemistry and colloidal stability. These insights enabled the preparation of stable naked NC inks of desorption-susceptible NC compositions such as PbSe, which were easily assembled into new mesostructured films and polymer-nanocrystal composites with wide-ranging technological applications.

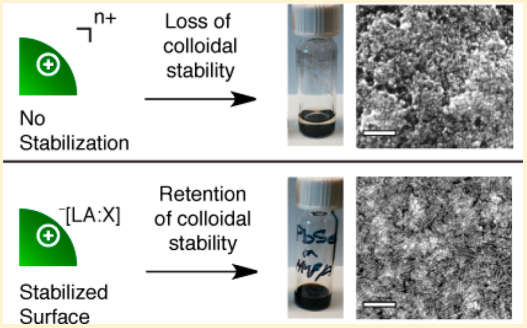

INTRODUCTION

Mesoscale chemistry increasingly relies on the assembly of preformed nanoscale building units into ordered hybrid architectures.[1−5] The surface chemistry of the building units strongly influences their assembly trajectory from spatially random to periodically ordered mesostructures, which in turn allows one to engineer new properties from the coupled interactions among components in the material.[6−15] Colloidal nanocrystals (NCs) are versatile building units in this regard. As synthesized, they typically feature a dense packing of hydrophobic organic ligands chemisorbed to the NC's inorganic surface. We and others have shown previously that, in order to assemble NCs into ordered mesostructured materials, particularly at high volume fractions, their surfaces must first be transformed chemically to enable favorable interactions with block copolymer (BCP) architecture-directing agents.[16−24] Understanding the mechanistic origins and outcomes that allow NC surfaces to be primed for BCP-directed assembly is therefore critical to advancing the emerging field of mesoscale science.

Despite the growing number of useful ligand exchange and ligand stripping chemistries now available,[25−44] we are only beginning to understand the mechanistic underpinnings of those transformations.[27,31,40,45−50] It is still difficult to explain and predict trends in reactivity for different NC compositions for a given transformation. For example, some NC compositions have not been amenable to native ligand removal while also maintaining colloidal dispersibility—e.g., the lead chalcogenides.[38,51] Disparities in surface reactivity and stability are related to structure and bonding available to the material and demand that we develop an arsenal of reagents that can be tailored as needed for the desired transformation of a NC of interest.

In the past, we and others have used irreversible chemical reactions, including alkylation with Meerwein's salt or oxidation by the nitrosyl cation, to drive the removal of ligands from NC surfaces.[33,38,51] These reactions yield charge-stabilized colloids in polar dispersants due to open metal coordination sites left at the NC surface following ligand stripping (Scheme 1a). Chemical approaches based on such irreversible reactions leave behind a transiently unstable surface (i.e., absent any stabilizing adsorbates), which can lead to desorption of excess metal cations from the surface and loss of dispersibility (due to loss of surface charge) on a time scale similar to repassivation with coordinating solvent.

Received: August 22, 2014
Published: October 10, 2014

   dx.doi.org/10.1021/ja508675t | J. Am. Chem. Soc. 2014, 136, 15702−15710

Scheme 1. Mechanistic Grounds Distinguishing Various Native Ligand Stripping Chemistries That Yield Cationic Naked NCs:[a] (a) Irreversible Ligand Stripping by Strong Electrophiles Yielding a Cationic NC Surface with No Electrostatic Stabilization;[b] (b) Ligand Stripping under Equilibrium Control Stabilizing the Cationic NC Surface through Dynamic Interactions with an Anionic Physisorbed Species $[LA:X]^-$ until It Can Be Repassivated with L[c]

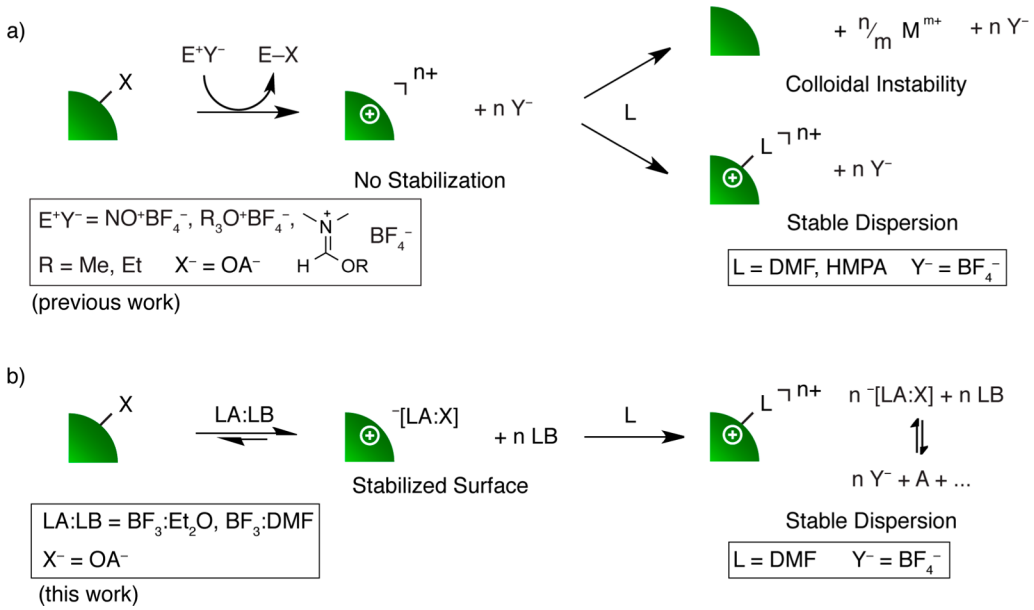

[a]Abbreviations: X^- = anionic ligand, E^+ = electrophile, Y^- = non-coordinating anion, M^{m+} = metal ion, LA:LB = Lewis acid–base adduct, L = charge-neutral coordinating solvent (e.g., DMF). [b]For sensitive NC compositions, loss of M^{m+} from the surface leads to colloidal instability, particularly when repassivation of surface M^{m+} by L is not competitive with M^{m+} desorption. [c]The dynamic exchange of $[LA:X]^-$ on and off the NC differentiates stripping under equilibrium control from earlier approaches. In the approach described herein, Y^- is generated through disproportionation of $[LA:X]^-$ as described in the main text.

We hypothesized that this undesirable outcome could be avoided if it were possible to stabilize the NC surface through the entire ligand-stripping pathway. Here, we introduce the concept of native ligand stripping under equilibrium control, where reversible Lewis acid–base chemistry is used to generate adduct-stabilized surfaces during ligand stripping (Scheme 1b). The dynamic exchange of these adducts on and off the NC surface allows for ligand displacement while imparting surface stabilization, in contrast to previous approaches that leave the surface without stabilization. Our concept of equilibrium control over ligand stripping is demonstrated using Lewis base adducts of BF_3, which yield for the first time naked NC inks of PbSe, along with a wide range of other semiconductor and metallic NCs. Our analysis of excess surface Pb(II) before and after stripping under equilibrium control indicated near-complete retention of excess Pb(II), in contrast with irreversible ligand stripping approaches. To rationalize differences in ligand-stripping outcomes with different reagents, we investigated in detail the mechanism of oleate ligand removal from PbSe NCs using complementary in situ techniques, including both 1D and 2D nuclear magnetic resonance (NMR) spectroscopy for both ^{1}H- and ^{19}F-containing reaction intermediates, as well as electrospray ionization mass spectrometry (ESI-MS) in order to validate our structure assignments.

Unique to the chemistry developed herein, we show that BF_3 reacts with the carboxylate terminus of PbSe-bound oleate ligands (OA^-) to form a physisorbed $[OA:BF_3]^-$ adduct that is in dynamic exchange (equilibrium) on and off the NC surface throughout the stripping reaction. We reason that this dynamic layer of $[OA:BF_3]^-$ at PbSe is responsible for the observed surface stabilization and refer to this effect as equilibrium control over surface stabilization. We further show that anionic $[OA:BF_3]^-$ undergoes disproportionation reactions in the presence of excess BF_3, ultimately leading to the loss of oleate as neutral $OA_x(B_yF_z)$ species and the formation of BF_4^- as the sole charge-compensating species at the cationic NC surface in the final naked nanocrystal dispersion. The quality of these nanoinks allows PbSe NCs to be assembled into either single-component ordered NC films or periodic mesostructured composites using block copolymer directed assembly, highlighting the versatility of these functional nanoscale building units in mesoscale chemistry.

RESULTS AND DISCUSSION

As a test case to highlight the versatility of native ligand stripping under equilibrium control over previously reported procedures, we investigated in detail the removal of oleate ligands from the surface of PbSe NCs (PbSe-OA) using Lewis base adducts of BF_3. As Se^{2-} in the NC lattice is easily oxidized, PbSe NCs require mild chemical reagents to strip them of their native ligands. While reagents such as trialkyloxonium salts (e.g., Meerwein's salt) and 1-alkoxy-*N*,*N*-dimethylmethaminium salts have so far proven capable of stripping ligands from the NC surface, by either method, the resulting naked PbSe NCs are not dispersible in organic solvents.[38,51] Both alkylating agents are high-energy reactants, and their use is commensurate with rapid and irreversible removal of chemisorbed organic ligands from NC surfaces. For NCs such as PbSe, loss of native ligands from the coordination sphere of surface Pb(II) can lead to desorption of Pb(II) from the NC surface. Here, we show that by changing the ligand-stripping chemistry to one that

dx.doi.org/10.1021/ja508675t | J. Am. Chem. Soc. 2014, 136, 15702–15710

allows for equilibrium control over surface stabilization, we are able to completely avoid loss of surface Pb(II) and thereby preserve colloidal stability in the cationic naked PbSe NC inks.

Stable dispersions of cationic naked PbSe NCs with BF_4^- counterions were obtained by direct transfer of PbSe-OA into *N*,*N*-dimethylformamide (DMF) containing BF_3:Et_2O. The resulting PbSe dispersions—purified first by hexane washes and then precipitation from DMF with toluene—were stable to centrifugation and filtration for days. The efficient removal of ligands by Lewis base adducts of BF_3 (BF_3:LB) was confirmed by FT-IR and EDX, which showed a dramatic decrease in intensity of the C−H vibrational stretching frequencies and carbon content, respectively (Figures S1 and S2 (Supporting Information)). Ligand removal was further verified by carrying out the stripping procedure in DMF-d_7 and acquiring the ^{1}H NMR spectrum (Figure S3), which showed no residual oleate. In order to establish the compositional diversity afforded by ligand stripping under equilibrium control, we showed that charge-stabilized dispersions of naked ZnO, Mn_3O_4, TiO_2, and Ni can be prepared in a manner similar to that described for PbSe (Figures S4 and S5). Despite the dramatic change in NC surface chemistry, we did not observe dramatic changes in size or crystal structure, as evidenced by TEM and XRD (Figures S5 and S6). Thus, this approach efficiently removes organic ligands from NC surfaces while preserving the integrity of the inorganic NC core.

In order to understand the microscopic chemical processes leading to stable dispersions of naked PbSe NCs, we followed the ligand-stripping chemistry of PbSe-OA in situ in toluene-d_8 using diffusion-ordered spectroscopy (DOSY). DOSY is a 2D NMR technique that provides information about the chemical shifts and diffusion coefficients of NMR-active species and has been used to identify and track the dynamics of ligand exchange (but not stripping) on a variety of NC surfaces.[46,47,50,52−54] The ^{1}H DOSY spectrum of 6.8 ± 0.5 nm PbSe-OA NCs (Figure S7) showed broad peaks with chemical shifts characteristic of bound oleate and a diffusion coefficient of (0.75 ± 0.01) × 10^{-10} m^2 s^{-1}. This contrasts significantly with the diffusion coefficient of free oleic acid of (7.75 ± 0.05) × 10^{-10} m^2 s^{-1} (Figure S8). The measured diffusion coefficient for PbSe-OA corresponds to a hydrodynamic diameter of 10.0 ± 0.5 nm, which agrees well with a 6.8 nm PbSe core and a tightly bound ∼1.6 nm ligand shell on each side.

The broad alkene resonance at δ 5.7 ppm is well separated from other resonances in the ^{1}H NMR spectrum and provides an ideal handle for tracking the fate of oleate as ligand stripping progresses. As BF_3:Et_2O was added to the NC dispersion, the broad oleate alkene resonance shifted upfield and decreased in intensity while a sharp resonance at δ 5.4−5.5 ppm, which we assign to $[OA:BF_3]^-$, appeared and grew in intensity (Figure 1a). The measured diffusion coefficient of the broad resonance increased only slightly throughout the experiment (from (0.75 ± 0.01) × 10^{-10} to (1.20 ± 0.02) × 10^{-10} m^2 s^{-1}), but the measured diffusion coefficient of the sharp resonance increased from (1.02 ± 0.03) × 10^{-10} m^2 s^{-1} at 0.2 equiv of BF_3 to (4.43 ± 0.02) × 10^{-10} m^2 s^{-1} at 2.3 equiv of BF_3 (Figure 1b and Figure S9). This can be explained by oleate reacting with BF_3:Et_2O to form $[OA:BF_3]^-$ and Et_2O. As the negative charge of $[OA:BF_3]^-$ is more diffuse than that of OA^-, $[OA:BF_3]^-$ is expected to bind much less strongly to the nanocrystal surface. As a result, $[OA:BF_3]^-$ rapidly exchanges on and off the nanocrystal, and the observed diffusion coefficient is a weighted average between the bound and unbound states.

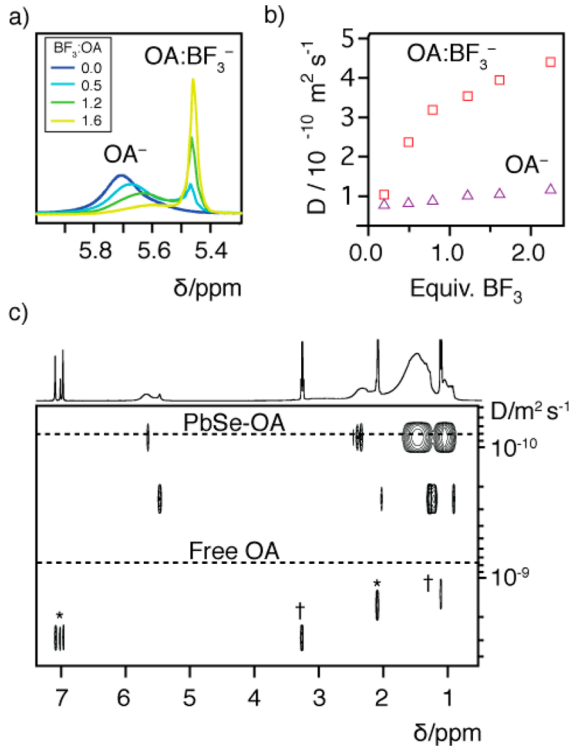

Figure 1. Titration of PbSe-OA in toluene-d_8 with BF_3:Et_2O: (a) ^{1}H spectra of the alkene resonance of oleate after addition of 0, 0.5, 1.2, and 1.6 equiv (with respect to oleate) of BF_3:Et_2O; (b) measured diffusion coefficient for the broad (OA^-) and sharp ($[OA:BF_3]^-$) resonances as a function of added BF_3:Et_2O; (c) Representative DOSY plot of PbSe-OA + 0.5 equiv of BF_3:Et_2O. For clarity, integration regions for the DOSY spectrum were manually defined to avoid regions where overlapping peaks led to artifacts in the DOSY spectrum. Dashed lines corresponding to the diffusion coefficients of PbSe-OA and free oleic acid, measured separately, are included for comparison. Asterisks (*) indicate solvent, and daggers (†) indicate Et_2O.

As the titration proceeded, $[OA:BF_3]^-$ became increasingly liberated from the surface. On the other hand, unreacted oleate remained tightly bound to the NC. As more of the ligand shell was removed, the remaining oleate ligands experienced more configurational entropy (or conformational degrees of freedom), allowing them to reconfigure at the ligand−NC interface. As a result, the hydrodynamic diameter of the NC, as measured by DOSY of the broad resonance at δ 5.7 ppm, decreased from 10.0 ± 0.5 nm (inorganic core + ligand shell) to 6.3 ± 0.3 nm (inorganic core alone) over the course of the titration. Changes in the chemical shift for tightly bound oleate can be explained by changes in the local dielectric environment as neighboring oleate ligands are removed. These results provide strong support that $[OA:BF_3]^-$ adducts are exchanging on and off the surface of PbSe nanocrystals during the stripping process, thus stabilizing the surface against surface metal cation desorption. Alternate explanations for the sharp peak at δ 5.5 ppm were considered but found to be inconsistent with our observations. For example, we considered that the sharp resonance at δ 5.5 ppm could be due to the exchange of charge-neutral $Pb(OA)_2$, which Hens and co-workers observed in the case of PbSe-OA oxidation.[46] However, we found that $Pb(OA)_2$ is unstable in the presence of BF_3, making this hypothesis unlikely (Figure S10). Furthermore, all experiments were carried out in tightly sealed screw-top NMR tubes, which were immediately transferred

dx.doi.org/10.1021/ja508675t | J. Am. Chem. Soc. 2014, 136, 15702−15710

from a glovebox into the NMR spectrometer in order to avoid oxygen exposure. We also ruled out the possibility that $[OA:BF_3]^-$ was merely becoming entangled in the ligand shell rather than exchanging on and off the nanocrystal surface by considering that the diffusion coefficient measured at 2.3 equiv of added BF_3:Et_2O indicated that the species was still spending some time diffusing with the nanocrystal, despite the almost complete loss of the ligand shell at this point in the titration.

Support that BF_3:Et_2O-mediated equilibrium-controlled ligand stripping avoids loss of surface excess Pb(II) was provided by measurement of the PbSe NC's surface excess Pb(II) before and after stripping using inductively coupled plasma atomic emission spectroscopy (ICP-AES). As-synthesized 5.8 ± 0.5 nm diameter PbSe-OA NCs gave a Pb:Se ratio of 1.24 ± 0.03, while naked PbSe returned with a 1.23 ± 0.02 Pb:Se ratio. This retention of surface excess Pb(II) during ligand stripping is unique among agents that generate naked PbSe nanocrystals: a ∼1:1 ratio is typically observed when using Meerwein's salt directly, while a 1.15:1 ratio is observed when using 1-ethoxy-*N*,*N*-dimethylmethaminium tetrafluoroborate.[51] Moreover, our new BF_3:LB approach is the only procedure that yields dispersible naked PbSe, most likely due to the enhanced electrostatic stabilization that follows retention of excess surface Pb(II). On the basis of these data, it is then appropriate to describe the composition of naked PbSe nanocrystals as $(Pb^{2+})_{0.23n}(Y^-)_{0.46n}(PbSe)_n$, where n is ∼1600 and Y^- is the counterion generated during ligand stripping.[55]

Given that no exogenous ions of the type Y^- were added to the ligand-stripping solution, it was necessary to establish the chemical identity of Y^- and its mechanistic origins as the compensating charge at the cationic naked PbSe NC surface. FT-IR of a thin film of naked PbSe NCs showed a strong peak at 1120 cm^{-1}, suggesting the presence of BF_4^- even though no BF_4^- was added to the ligand-stripping solution. To confirm that BF_4^- was present in the purified dispersions of naked PbSe NCs, ^{19}F NMR was carried out. Strong peaks at δ −151.72 and −151.77 ppm with a 1:4 ratio in integrated intensity were observed, consistent with isotopic shifts due to bonding of ^{19}F to ^{10}B and ^{11}B, respectively (Figure 2). The assignment of this peak to BF_4^- was made by acquiring the ^{19}F NMR spectrum of $NaBF_4$ in DMF and noting a chemical shift similar to that observed for our naked PbSe dispersions (Figure 2a,b). We also noted that BF_4^- in naked PbSe dispersions is only weakly, if at all, associating with the NC surface in DMF (Figure 2c,d).

In order to establish the origins of the formation of BF_4^-, we acquired the ^{19}F NMR spectrum for BF_3:Et_2O in DMF-d_7 (Figure S11). The major chemical species present was the DMF adduct of BF_3 at δ −152.4 ppm, this adduct accounting for 96% of the fluorine in the system, alongside two minor fluorine-containing species. The chemical shifts of these minor species were δ −150.8 and −151.8 ppm and were present in an ∼1:2 ratio in integrated intensity. On the basis of the chemical shift, the peak at δ −151.8 ppm can be assigned to BF_4^-. These data are consistent with the disproportionation of DMF:BF_3 to form $[(DMF)_2BF_2]^+$ and BF_4^-, thus accounting for one possible source of BF_4^- counterions in naked PbSe NC dispersions (Scheme 2).[56]

From the view of electroneutrality, the replacement of anionic oleate ligands with non-coordinating BF_4^- counterions at the NC surface requires both generation of BF_4^- and either conversion of oleate anions to a neutral species or pairing of oleate with a cationic species (i.e., OA^- with $[(DMF)_2BF_2]^+$).

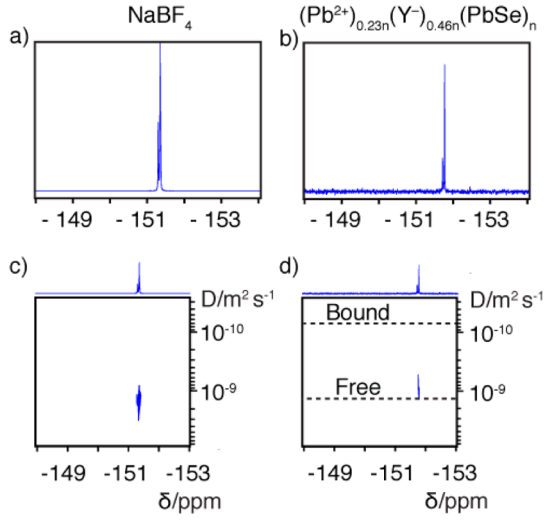

Figure 2. ^{19}F NMR evidence for BF_4^- as a non-coordinating counterion in naked PbSe NC dispersions. ^{19}F NMR spectra of (a) $NaBF_4$ and (b) naked PbSe NC in DMF. Identification of the species as BF_4^- was made on the basis of similar chemical shifts. The slight difference in chemical shifts can be attributed to concentration and dielectric effects. ^{19}F-DOSY spectra for (c) $NaBF_4$ and (d) naked PbSe NC in DMF. On the basis of these data, it is clear that BF_4^- is only weakly, if at all, associating with the NC surface in this high dielectric constant dispersant.

Scheme 2. Disproportionation of DMF:BF_3[a]

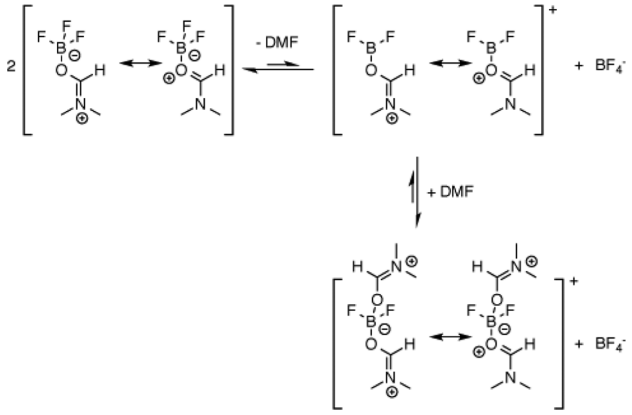

[a]DMF:BF_3 initially forms via an exchange of BF_3 from the weaker Lewis base diethyl ether to the more basic DMF (not shown). The DMF:BF_3 adduct is resonance stabilized. This adduct can react with a second equivalent of BF_3:DMF in a fluoride transfer reaction to yield BF_4^- and $[BF_2DMF]^+$. Finally, the open coordination site on boron is filled by DMF to yield $[BF_2(DMF)_2]^+$.

We sought to understand oleate speciation post-stripping by performing ESI-MS on a reaction mixture of $Pb(OA)_2$ and BF_3:Et_2O in benzene-d_6 (Figure 3). It is known from previous work that carboxylates can coordinate 1 or 2 equiv of BF_3 and that carboxylate BF_3 adducts can undergo disproportionation reactions to generate BF_4^- and $[B(O_2CR)_nF_{4-n}]^-$.[57] In accordance with this known reactivity pathway, ESI-MS indicated that our reaction mixture contained OA^- (**1**, m/z 281.25, calcd 281.25), $[OA:BF_3]^-$ (**2**, m/z 349.26, calcd 349.25), $[OA(BF_3)_2]^-$ (**3**, m/z 417.26, calcd 417.26), and $[B(OA)_2F_2]^-$ (**4**, m/z 611.50, calcd 611.50) (Scheme 3, Figure 3). In addition to anionic disproportionation products, we also observed species that resulted from the hydrolysis of neutral

dx.doi.org/10.1021/ja508675t | J. Am. Chem. Soc. 2014, 136, 15702−15710

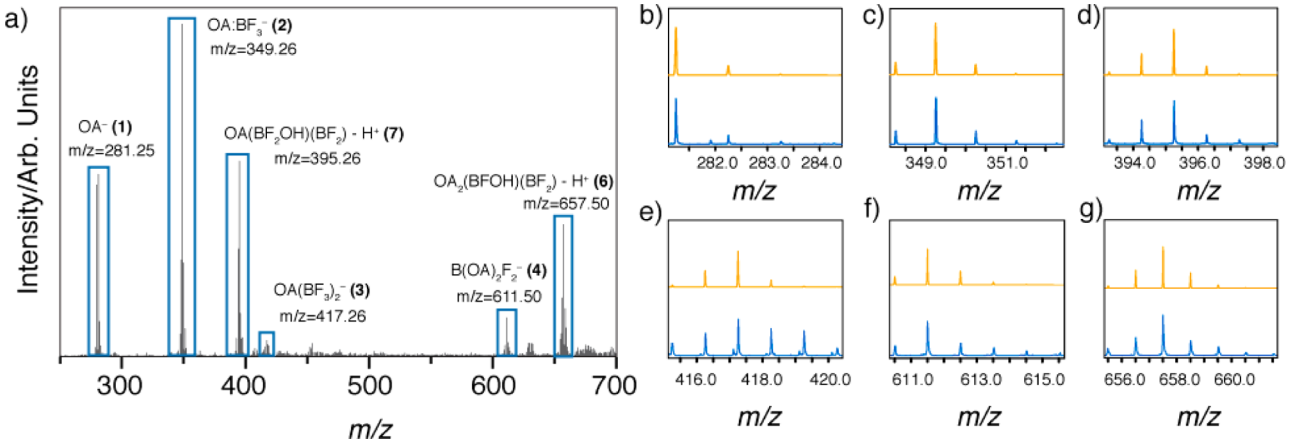

Figure 3. (a) High-resolution negative-ion mode ESI-MS of $Pb(OA)_2$ + BF_3:Et_2O. Six of the species proposed in Scheme 3 were identified in the mass spectrum and are boxed for clarity. Isotope distribution patterns for (b) OA^-, (c) $[OA:BF_3]^-$, (d) $[OA(BF_2)(BF_2O)]^-$, (e) $[OA(BF_3)_2]^-$, (f) $[B(OA)_2F_2]^-$, and (g) $[(OA)_2(BF_2)(BFO)]^-$ are shown in blue (bottom trace) along with predicted patterns (orange, top trace). Fully annotated isotope distribution patterns can be found in (Figure S12).

Scheme 3. Reaction Pathways Available to OA^- in the Presence of BF_3:Et_2O to Yield BF_4^-[a]

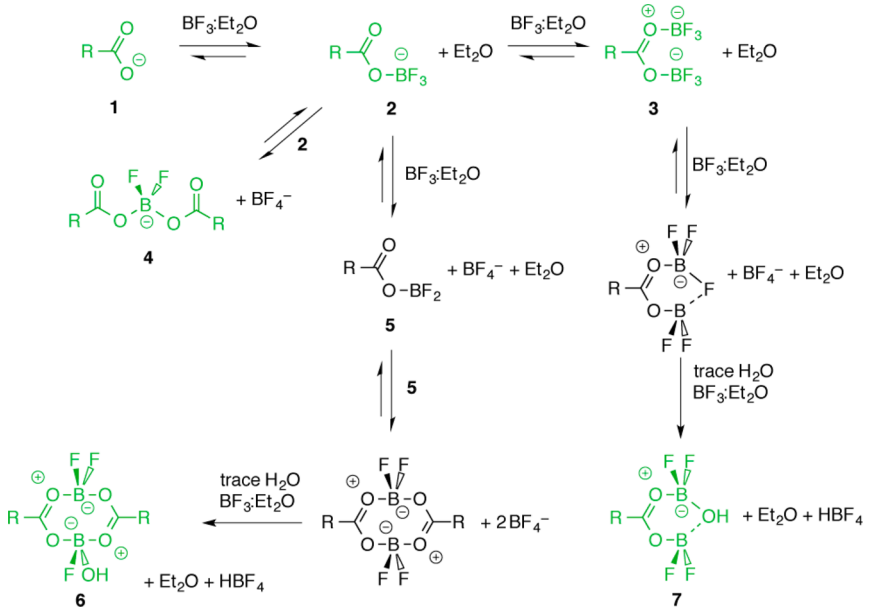

[a]OA^- forms adducts with either 1 or 2 equiv of BF_3 to give intermediates **2** and **3**, respectively. Compound **2** undergoes disproportionation, yielding $[B(OA)_2F_2]^-$ and BF_4^-. Alternatively, **2** can transfer a fluoride to BF_3:Et_2O to give the charge-neutral species **5** and BF_4^-. Species **5** dimerizes readily and is observable as compound **6** in the presence of adventitious H_2O during the ESI-MS measurements. BF_3-mediated disproportionation of **3** is also observable along the reaction pathway proposed. Chemical structures for **1**–**4**, **6**, and **7** (in green) were verified by ESI-MS.

disproportionation products in the presence of adventitious water. For example, fluoride transfer from $[OA:BF_3]^-$ (**2**) to BF_3:Et_2O generates BF_4^- and $OA(BF_2)$ (**5**), which readily dimerizes to form the neutral $(OA)_2(BF_2)_2$ species. While this dimer is not directly observable by ESI-MS due to its lack of charge, the deprotonated hydrolysis product $[(OA)_2(BF_2)(BFO)]^-$ (**6**, *m*/*z* 657.50, calcd 657.51) was observed. The $[OA(BF_3)_2]^-$ adduct **3** can also undergo fluoride loss to generate BF_4^- and neutral $OA(BF_3)(BF_2)$. Again, this neutral species is undetectable by ESI-MS, but we observed the deprotonated form of the hydrolysis product, $[OA(BF_2)(BF_2O)]^-$ (**7**, *m*/*z* 395.26, calcd 395.26). The transfer of fluoride from BF_3 oleate adducts to excess BF_3:Et_2O provides a pathway for the conversion of anionic oleate ligands into neutral species along with the generation of non-coordinating BF_4^-. It is also worth noting that, in addition to $[OA:BF_3]^-$, the anionic species formed along this pathway also have the ability to stabilize NC surfaces during the stripping process.

The unprecedented access to stable dispersions of cationic naked PbSe NCs allowed us to better control their mesoscale order in thin films and composites, yielding new classes of mesostructured materials with applications as energy conversion materials. For example, thin films of lead chalcogenide NCs are common active layers in Schottky-type solar cells, field effect transistors, NIR photodetectors, and thermoelectrics.[25,30,36,51,58−66] As synthesized (i.e., with ligands intact), they can be assembled into periodic lattices with hexagonal close packing (*hcp*). Where controlled propagation of energy in the film is required for the function of the device, ligand removal can be advantageous. As shown here and elsewhere,

dx.doi.org/10.1021/ja508675t | J. Am. Chem. Soc. 2014, 136, 15702−15710

order is usually lost upon stripping ligands in thin films (Figure 4 and (Figure S13).[25,67] In addition, cracks and defects can

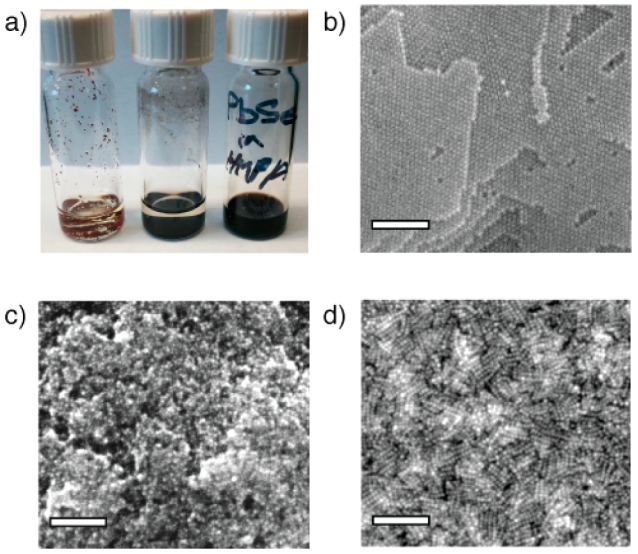

Figure 4. (a) Comparison of different ligand stripping reagents for PbSe-OA: (left) rapid oxidation of PbSe by $NOBF_4$ to yield the red allotrope of Se^0; (middle) application of Meerwein's salt to yield stoichiometric PbSe with poor dispersibility; (right) ligand stripping with Lewis base adducts of BF_3 to yield stable dispersions of cationic naked PbSe NCs; (b) Formation of PbSe-OAs *hcp* superlattices on deposition from stable dispersions in aliphatic hydrocarbons; (c) In-film removal of oleates in *hcp*-ordered PbSe-OA films by Lewis base adducts of BF_3 destroys ordering and introduces cracking; (d) Film deposition from cationic naked PbSe NC inks to yield large-area, ordered films with improved film quality. All scale bars are 100 nm.

manifest as a result of the dramatic volume change that occurs when organics are liberated. In contrast to the colloidal glasses produced by in-film ligand removal, ordered thin films of naked PbSe can be prepared simply by casting their dispersions directly onto substrates. Apparent cubic packing is evidenced in the top-down SEM images (Figure 4d), indicating significant differences in the preferred packing geometry for ligand-coated and ligand-stripped NCs. To further distinguish packing geometries between the different PbSe NC films, grazing incidence small-angle X-ray scattering (GISAXS) was carried out. Both ligand-stripped PbSe NC films in Figure 4c,d showed a decrease in interparticle spacing from ~1.3 to ~0.4 nm, consistent with ligand removal. However, films that were spin-coated from stripped dispersions of PbSe exhibited a tendency toward in-plane ordering as opposed to the isotropic packing observed in films that were stripped in-film (Figure 4d and Figure S13).

The observed packing in films deposited from ligand-coated vs ligand-stripped PbSe NCs can arise from differences in surface energies of exposed facets leading to preferred NC-to-NC orientations,[68] differences in packing preferences for nondeformable objects (i.e., the naked PbSe) in comparison to partially deformable ligand-coated particles,[69] and differences in interaction potentials available to the system to guide the assembly trajectory during solvent evaporation (van der Waals vs electrostatics).[70] As such, our work suggests new opportunities to control energy propagation in NC films through their packing in the active layers.

More elaborate mesostructured BCP-NC hybrid architectures were also possible using polystyrene-*block*-poly(*N*,*N*-dimethylacrylamide) architecture-directing agents.[20] For example, naked NC inks of PbSe were mixed with architecture-directing BCPs and deposited onto Si substrates by drop casting or spin coating to prepare hierarchically ordered composites (Figure 5). Notably, no further thermal or solvent

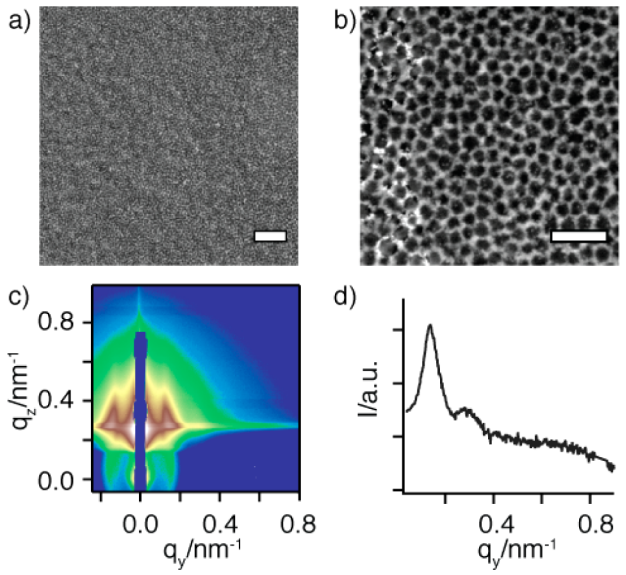

Figure 5. PbSe polymer composites deposited directly from solution: (a, b) top-down SEM of a composite at increasing magnification, with scale bars of (a) 500 and (b) 200 nm; (c) GISAXS pattern taken at an incident angle of 0.16° and sample−detector distance of 3.9 m; (d) line scan along the q_y axis of the GISAXS pattern.

vapor treatment of the films was required to establish order. As measured by GISAXS, these composites exhibited an in-plane periodicity of 45 nm, with a peak width at half-maximum of 0.008 $Å^{-1}$. These new materials were only accessible thanks to the improved control over surface chemistry granted by our new chemical approach, and the availability of naked NC inks of PbSe opens the door to creating a wide variety of new and interesting mesoscale architectures that have been impossible in the past.

■ CONCLUSIONS

The mechanistic insights gained in this work provide a much-needed framework for rationalizing the successes and failures of different chemical approaches for removing surface-bound ligands from nanocrystals while maintaining colloidal dispersibility. We hypothesized that earlier approaches based on irreversible severing of NC−ligand bonds failed to maintain colloidal dispersibility for sensitive compositions due to a lack of surface stabilization and concomitant desorption of excess metal cations from the NC surface. To address this shortcoming, we proposed the use of reversible Lewis acid−base chemistry to generate physisorbed anionic species that stabilize the NC surface until coordinating solvent is able to repassivate the surface. Using PbSe NC as a model system, we demonstrated that anionic BF_3 adducts of surface-bound ligands exchanged on and off the NC surface, providing stabilization. Furthermore, we showed that NCs stripped under equilibrium control maintained colloidal stability and did not suffer from the excess surface metal desorption that can be

problematic when using some irreversible ligand stripping reagents. As a result, ligand stripping under equilibrium control represents a powerful new class of reactions for modifying the surface chemistry of colloidal NC while maintaining colloidal stability.

We leveraged this additional control to prepare previously unobtainable mesostructured NC films and polymer-NC composites with high mass loadings of PbSe. Notably, these composites did not require any further thermal or solvent-vapor treatment to establish order, which simplifies their processing for final applications, including photovoltaics, thermoelectrics, and NIR photodetectors. These new materials are expected to yield insights into the role of architecture on electronic, excitonic, and thermal transport in mesostructured materials and composites.

EXPERIMENTAL SECTION

Materials and Methods. Acetone (anhydrous, 99.9%), benzene-d_6 (99.6% atom D), 1,4-dioxane (anhydrous, 99.8%), diphenylphosphine (98%), ethanol (anhydrous, 99.5%), hexamethylphosphoramide (HMPA, 99%), hexanes (anhydrous, 99%), lead(II) nitrate (99.99%), lead(II) oxide (99.999% trace metals grade), *N*,*N*-dimethylformamide (anhydrous, 99.8%), *N*,*N*-dimethylformamide-d_7 (99.5% atom D), nitric acid (70%, 99.999% trace metals grade), 1-octadecene (90% tech grade), octane (anhydrous, 99%), oleic acid (90% tech grade), selenium shot (99.999% trace metals grade), toluene (anhydrous, 99.8%), toluene-d_8 (99.6% atom D), and α,α,α-trifluorotoluene (anhydrous, 99%) were obtained from Sigma-Aldrich. Boron trifluoride etherate (BF_3:Et_2O, 48% BF_3 basis) was obtained from Acros Organics. Tri-*n*-octylphosphine (TOP, 90% tech grade) was obtained from Alfa Aesar. Pb and Se standards for ICP-AES were obtained from Fluka. Sodium oleate (97%) was obtained from Pfaltz & Bauer. All chemicals were used as received. Lead oleate was prepared by metathesis of lead(II) nitrate and sodium oleate. NMR spectra were acquired on a Bruker Biospin 500 MHz NMR spectrometer at 500 MHz for ^{1}H and 470 MHz for ^{19}F. ^{1}H chemical shifts were referenced with respect to residual solvent peaks, and ^{19}F shifts were internally referenced to α,α,α-trifluorotoluene (−63.72 ppm from $CFCl_3$) as a secondary standard. Pb and Se contents of NC samples were measured by ICP-AES on a Varian 720-ES spectrometer using an argon plasma. Prior to analysis, dried NC samples were digested in 70% nitric acid in a closed Teflon container for several days. High-resolution ESI-MS spectra were obtained in negative ion mode on a Bruker microTOF Q high-resolution mass spectrometer. SEM images were obtained with a Zeiss Gemini Ultra-55 analytical scanning electron microscope equipped with in-lens and secondary electron detectors at a beam energy of 2−5 keV. Grazing incidence small-angle X-ray scattering measurements were made at beamline 7.3.3 of the Advanced Light Source, Lawrence Berkeley National Laboratory, using an incident angle of 0.16°, a wavelength of 0.124 nm (10 keV), a detector distance of 3.9 m, and recorded on a Pilatus 1 M flat detector.[71] The resulting data were processed with the Nika 2D SAS software package in Igor Pro.[72]

Synthesis of Oleate-Passivated Lead Selenide Nanocrystals (PbSe-OA). Lead selenide nanocrystals were synthesized under an inert atmosphere following slightly modified reported procedures.[73] Briefly, selenium shot (960 mg, 12.2 mmol) was added to TOP (8.64 g, 23.3 mmol) in a 40 mL septum-capped vial and the mixture was stirred overnight in a nitrogen glovebox prior to the addition of diphenylphosphine (84 mg, 0.45 mmol). Separately, in a 100 mL three-necked flask, lead(II) oxide (1.34 g, 6 mmol), oleic acid (4.24 g, 15 mmol), and 1-octadecene (23.4 mL) were placed under vacuum at room temperature for 15 min and then at 110 °C for 1 h to dry and degas the solution. After the solution became colorless and transparent, the temperature was raised to 180 °C under N_2, at which point the TOP-Se solution was rapidly injected. After this TOP-Se injection, the reaction temperature was dropped to ∼150 °C and was kept at this temperature for the desired reaction time (5 min gave PbSe nanocrystals with ∼7 nm diameter). The reaction mixture was cooled in a water bath. The nanocrystals were then purified by precipitation three times from hexanes using first ethanol (1×) and then acetone (2×) to give 460 mg of purified NC (1.2 mmol of $(PbOA)_{0.2}PbSe$, 24% yield).

Ligand Stripping Procedure. Activated DMF was prepared in a nitrogen glovebox by adding BF_3:Et_2O (20 μL, 0.16 mmol) to 500 μL of DMF and mixing vigorously. Next, 500 μL of a stock solution of nanocrystals in hexanes (5−10 mg mL^{-1}) was added to the activated DMF and the mixture was mixed vigorously. Toluene (3.5 mL) was then added to induce mixing of the two layers and precipitation of stripped nanocrystals, which were redispersed in DMF. The resulting naked nanocrystal dispersion was purified by multiple washes with hexanes and precipitation from DMF with toluene.

In Situ NMR. A known amount of PbSe-OA was dried under vacuum and redispersed in toluene-d_8. The amount of oleate in the system was determined by quantitative NMR using 1,4-dioxane as an internal standard and 45 s interscan delays. Diffusion ordered spectroscopy (DOSY) was carried out at room temperature using standard bipolar convection compensating pulses. The diffusion delay, Δ, was set to 200 ms and the gradient pulse length, δ, was set to achieve at least 90% signal attenuation between 95% and 5% gradient strength. For the BF_3 titration experiment, the gradient pulse length was held at 5 ms, but for other experiments it varied from 1 to 2 ms. The gradient strength was varied between 5 and 95% of the calibrated maximum gradient strength of 51.1 G cm^{-1} in 16 steps. The resulting data were processed in the Bruker Topspin and Bruker Dynamics Center software packages, where it was fit to the appropriate form of the Stejskal−Tanner equation.

ESI-MS. A reaction mixture of $Pb(OA)_2$ and BF_3:Et_2O was prepared by dissolving $Pb(OA)_2$ (3 mg, 4 μmol) in 700 μL of benzene-d_6 and adding BF_3:Et_2O (8 μmol). For improved ionization efficiency, the reaction mixture was diluted 5-fold with dry acetonitrile to prepare the final ESI-MS sample. ESI-MS was run in negative ion mode.

Preparation of Naked Nanocrystal Thin Films and Polymer Composites. Thin films of PbSe-OA were prepared by spin coating a solution of PbSe-OA in 1/1 hexane/octane onto a silicon wafer. To strip the NC film in the solid state, the film was dipped into a solution of BF_3:Et_2O (50 μL) in HMPA (1 mL) and rinsed with hexanes. Ordered thin films of naked PbSe NC could be prepared by spin coating a solution (∼10 mg mL^{-1}) of naked PbSe NC directly onto a silicon wafer. Architecture-directing 60 kDa−20 kDa PS-*b*-PDMA block copolymers were prepared as described by us elsewhere[20] and dissolved in DMF to form a stock solution at a concentration of 50 mg mL^{-1}. Separately, a 30 mg mL^{-1} stock solution of naked PbSe NC in DMF was prepared. The stock solutions were mixed along with excess DMF to yield a solution with a final concentration of 10 mg of polymer mL^{-1} and 3−10 mg of NC mL^{-1}, which was dropcast directly onto a Si wafer to produce ordered polymer-NC composites.

ASSOCIATED CONTENT

Supporting Information

Text and figures giving additional experimental details, FT-IR, EDX, ^{1}H and ^{19}F NMR spectra, ζ potential measurements, TEM, XRD, isotope distribution patterns, and GISAXS patterns. This material is available free of charge via the Internet at http://pubs.acs.org.

AUTHOR INFORMATION

Corresponding Author

*E-mail for B.A.H.: bahelms@lbl.gov.

Author Contributions

The manuscript was written through contributions of all authors. All authors have given approval to the final version of the manuscript.

Notes

The authors declare no competing financial interest.

■ ACKNOWLEDGMENTS

We thank N. Su and T. Williams for supplying Ni nanocrystals and block copolymer architecture-directing agents, respectively, A. Hexemer for assistance with GISAXS, P. Frischmann for assistance with ESI-MS, and L. Gerber for helpful discussions. All work with PbSe, TiO_2, ZnO, and Mn_3O_4 was performed by S.E.D., C.L., A.W.W., and B.A.H. C.L. and B.A.H. were supported by the Joint Center for Energy Storage Research, an Energy Innovation Hub funded by the U.S. Department of Energy, Office of Science, Office of Basic Energy Sciences. S.E.D. was supported by the Department of Defense through the National Defense Science & Engineering Graduate Fellowship program. J.J.L. and J.J.U. carried out all experiments with Ni and $Cu_{1.7}Se$, acknowledging support from the AFOSR MURI program under FA9550-12-1-0002. Portions of the work—including nanocrystal synthesis, characterization, and chemical transformations thereof—were carried out as User Projects at the Molecular Foundry, which is supported by the Office of Science, Office of Basic Energy Sciences, of the U.S. Department of Energy under Contract No. DE-AC02-05CH11231. GISAXS was carried out at Beamline 7.3.3 of the Advanced Light Source, which is supported by the Director of the Office of Science, Office of Basic Energy Sciences, of the U.S. Department of Energy under the same contract.

■ REFERENCES

(1) Thompson, R. B.; Ginzburg, V. V.; Matsen, M. W.; Balazs, A. C. *Macromolecules* **2002**, *35*, 1060−1071.
(2) Min, Y.; Akbulut, M.; Kristiansen, K.; Golan, Y.; Israelachvili, J. *Nat. Mater.* **2008**, *7*, 527−538.
(3) Orilall, M. C.; Wiesner, U. *Chem. Soc. Rev.* **2011**, *40*, 520−535.
(4) Kao, J.; Thorkelsson, K.; Bai, P.; Rancatore, B. J.; Xu, T. *Chem. Soc. Rev.* **2013**, *42*, 2654−2678.
(5) Milliron, D. J.; Buonsanti, R.; Llordes, A.; Helms, B. A. *Acc. Chem. Res.* **2014**, *47*, 236−246.
(6) Maier, J. *Nat. Mater.* **2005**, *4*, 805−815.
(7) Aricò, A. S.; Bruce, P.; Scrosati, B.; Tarascon, J.-M.; van Schalkwijk, W. *Nat. Mater.* **2005**, *4*, 366−377.
(8) Snyder, G. J.; Toberer, E. S. *Nat. Mater.* **2008**, *7*, 105−114.
(9) Zabet-Khosousi, A.; Dhirani, A.-A. *Chem. Rev.* **2008**, *108*, 4072−4124.
(10) See, K. C.; Feser, J. P.; Chen, C. E.; Majumdar, A.; Urban, J. J.; Segalman, R. A. *Nano Lett.* **2010**, *10*, 4664−4667.
(11) Wang, R. Y.; Tangirala, R.; Raoux, S.; Jordan-Sweet, J. L.; Milliron, D. J. *Adv. Mater.* **2012**, *24*, 99−103.
(12) Ong, W.-L.; Rupich, S. M.; Talapin, D. V.; McGaughey, A. J. H.; Malen, J. A. *Nat. Mater.* **2013**, *12*, 410−415.
(13) Dong, A.; Jiao, Y.; Milliron, D. J. *ACS Nano* **2013**, *7*, 10978−10984.
(14) Kaushik, A. P.; Lukose, B.; Clancy, P. *ACS Nano* **2014**, *8*, 2302−2317.
(15) Akselrod, G. M.; Prins, F.; Poulikakos, L. V.; Lee, E. M. Y.; Weidman, M. C.; Mork, A. J.; Willard, A. P.; Bulović, V.; Tisdale, W. A. *Nano Lett.* **2014**, *14*, 3556−3562.
(16) Warren, S. C.; Messina, L. C.; Slaughter, L. S.; Kamperman, M.; Zhou, Q.; Gruner, S. M.; DiSalvo, F. J.; Wiesner, U. *Science* **2008**, *320*, 1748−1752.
(17) Brezesinski, T.; Wang, J.; Polleux, J.; Dunn, B.; Tolbert, S. H. *J. Am. Chem. Soc.* **2009**, *131*, 1802−1809.
(18) Kim, J.; Green, P. F. *Macromolecules* **2010**, *43*, 10452−10456.
(19) Hur, K.; Hennig, R. G.; Escobedo, F. A.; Wiesner, U. *Nano Lett.* **2012**, *12*, 3218−3223.
(20) Buonsanti, R.; Pick, T. E.; Krins, N.; Richardson, T. J.; Helms, B. A.; Milliron, D. J. *Nano Lett.* **2012**, *12*, 3872−3877.
(21) Rauda, I. E.; Buonsanti, R.; Saldarriaga-Lopez, L. C.; Benjauthrit, K.; Schelhas, L. T.; Stefik, M.; Augustyn, V.; Ko, J.; Dunn, B.; Wiesner, U.; Milliron, D. J.; Tolbert, S. H. *ACS Nano* **2012**, *6*, 6386−6399.
(22) Rauda, I. E.; Saldarriaga-Lopez, L. C.; Helms, B. A.; Schelhas, L. T.; Membreno, D.; Milliron, D. J.; Tolbert, S. H. *Adv. Mater.* **2013**, *25*, 1315−1322.
(23) Kao, J.; Bai, P.; Lucas, J. M.; Alivisatos, A. P.; Xu, T. *J. Am. Chem. Soc.* **2013**, *135*, 1680−1683.
(24) Rivest, J. B.; Buonsanti, R.; Pick, T. E.; Zhu, L.; Lim, E.; Clavero, C.; Schaible, E.; Helms, B. A.; Milliron, D. J. *J. Am. Chem. Soc.* **2013**, *135*, 7446−7449.
(25) Talapin, D. V.; Murray, C. B. *Science* **2005**, *310*, 86−89.
(26) Law, M.; Luther, J. M.; Song, Q.; Hughes, B. K.; Perkins, C. L.; Nozik, A. J. *J. Am. Chem. Soc.* **2008**, *130*, 5974−5985.
(27) Owen, J. S.; Park, J.; Trudeau, P.-E.; Alivisatos, A. P. *J. Am. Chem. Soc.* **2008**, *130*, 12279−12281.
(28) Kovalenko, M. V.; Scheele, M.; Talapin, D. V. *Science* **2009**, *324*, 1417−1420.
(29) Tangirala, R.; Baker, J. L.; Alivisatos, A. P.; Milliron, D. J. *Angew. Chem., Int. Ed.* **2010**, *49*, 2878−2882.
(30) Zarghami, M. H.; Liu, Y.; Gibbs, M.; Gebremichael, E.; Webster, C.; Law, M. *ACS Nano* **2010**, *4*, 2475−2485.
(31) Caldwell, M. A.; Albers, A. E.; Levy, S. C.; Pick, T. E.; Cohen, B. E.; Helms, B. A.; Milliron, D. J. *Chem. Commun.* **2011**, *47*, 556−558.
(32) Llordes, A.; Hammack, A. T.; Buonsanti, R.; Tangirala, R.; Aloni, S.; Helms, B. A.; Milliron, D. J. *J. Mater. Chem.* **2011**, *21*, 11631−11638.
(33) Dong, A.; Ye, X.; Chen, J.; Kang, Y.; Gordon, T.; Kikkawa, J. M.; Murray, C. B. *J. Am. Chem. Soc.* **2011**, *133*, 998−1006.
(34) Nag, A.; Kovalenko, M. V.; Lee, J.-S.; Liu, W.; Spokoyny, B.; Talapin, D. V. *J. Am. Chem. Soc.* **2011**, *133*, 10612−10620.
(35) Fafarman, A. T.; Koh, W.-K.; Diroll, B. T.; Kim, D. K.; Ko, D.-K.; Oh, S. J.; Ye, X.; Doan-Nguyen, V.; Crump, M. R.; Reifsnyder, D. C.; Murray, C. B.; Kagan, C. R. *J. Am. Chem. Soc.* **2011**, *133*, 15753−15761.
(36) Tang, J.; Kemp, K. W.; Hoogland, S.; Jeong, K. S.; Liu, H.; Levina, L.; Furukawa, M.; Wang, X.; Debnath, R.; Cha, D.; Chou, K. W.; Fischer, A.; Amassian, A.; Asbury, J. B.; Sargent, E. H. *Nat. Mater.* **2011**, *10*, 765−771.
(37) Zhang, H.; Hu, B.; Sun, L.; Hovden, R.; Wise, F. W.; Muller, D. A.; Robinson, R. D. *Nano Lett.* **2011**, *11*, 5356−5361.
(38) Rosen, E. L.; Buonsanti, R.; Llordes, A.; Sawvel, A. M.; Milliron, D. J.; Helms, B. A. *Angew. Chem., Int. Ed.* **2012**, *51*, 684−689.
(39) Anderson, N. C.; Owen, J. S. *Chem. Mater.* **2013**, *25*, 69−76.
(40) Anderson, N. C.; Hendricks, M. P.; Choi, J. J.; Owen, J. S. *J. Am. Chem. Soc.* **2013**, *135*, 18536−18548.
(41) Zanella, M.; Maserati, L.; Leal, M. P.; Prato, M.; Lavieville, R.; Povia, M.; Krahne, R.; Manna, L. *Chem. Mater.* **2013**, *25*, 1423−1429.
(42) Dirin, D. N.; Dreyfuss, S.; Bodnarchuk, M. I.; Nedelcu, G.; Papagiorgis, P.; Itskos, G.; Kovalenko, M. V. *J. Am. Chem. Soc.* **2014**, *136*, 6550−6553.
(43) Norman, Z. M.; Anderson, N. C.; Owen, J. S. *ACS Nano* **2014**, *8*, 7513−7521.
(44) Zhang, H.; Jang, J.; Liu, W.; Talapin, D. V. *ACS Nano* **2014**, *8*, 7359−7369.
(45) Ji, X.; Copenhaver, D.; Sichmeller, C.; Peng, X. *J. Am. Chem. Soc.* **2008**, *130*, 5726−5735.
(46) Moreels, I.; Fritzinger, B.; Martins, J. C.; Hens, Z. *J. Am. Chem. Soc.* **2008**, *130*, 15081−15086.
(47) Fritzinger, B.; Capek, R. K.; Lambert, K.; Martins, J. C.; Hens, Z. *J. Am. Chem. Soc.* **2010**, *132*, 10195−10201.
(48) Morris-Cohen, A. J.; Vasilenko, V.; Amin, V. A.; Reuter, M. G.; Weiss, E. A. *ACS Nano* **2012**, *6*, 557−565.
(49) Peterson, M. D.; Jensen, S. C.; Weinberg, D. J.; Weiss, E. A. *ACS Nano* **2014**, *8*, 2826−2837.

(50) De Roo, J.; Van den Broeck, F.; De Keukeleere, K.; Martins, J. C.; Van Driessche, I.; Hens, Z. *J. Am. Chem. Soc.* **2014**, *136*, 9650−9657.
(51) Rosen, E. L.; Sawvel, A. M.; Milliron, D. J.; Helms, B. A. *Chem. Mater.* **2014**, *26*, 2214−2217.
(52) Kohlmann, O.; Steinmetz, W. E.; Mao, X.-A.; Wuelfing, W. P.; Templeton, A. C.; Murray, R. W.; Johnson, C. S., Jr. *J. Phys. Chem. B* **2001**, *105*, 8801−8809.
(53) Hens, Z.; Moreels, I.; Martins, J. C. *ChemPhysChem* **2005**, *6*, 2578−2584.
(54) Hens, Z.; Martins, J. C. *Chem. Mater.* **2013**, *25*, 1211−1221.
(55) Moreels, I.; Lambert, K.; De Muynck, D.; Vanhaecke, F.; Poelman, D.; Martins, J. C.; Allan, G.; Hens, Z. *Chem. Mater.* **2007**, *19*, 6101−6106.
(56) Hartman, J. S.; Ilnicki, E. I.; Shoemaker, J. A. W.; Szerminski, W. R.; Yuan, Z. *Can. J. Chem.* **1998**, *76*, 1317−1326.
(57) Brownstein, S.; Latremouille, G. *Can. J. Chem.* **1978**, *56*, 2764−2767.
(58) Konstantatos, G.; Howard, I.; Fischer, A.; Hoogland, S.; Clifford, J.; Klem, E.; Levina, L.; Sargent, E. H. *Nature* **2006**, *442*, 180−183.
(59) Luther, J. M.; Law, M.; Beard, M. C.; Song, Q.; Reese, M. O.; Ellingson, R. J.; Nozik, A. J. *Nano Lett.* **2008**, *8*, 3488−3492.
(60) Hillhouse, H. W.; Beard, M. C. *Curr. Opin. Colloid Interface Sci.* **2009**, *14*, 245−259.
(61) Choi, J. J.; Lim, Y.-F.; Santiago-Berrios, M. B.; Oh, M.; Hyun, B.-R.; Sun, L.; Bartnik, A. C.; Goedhart, A.; Malliaras, G. G.; Abruña, H. D.; Wise, F. W.; Hanrath, T. *Nano Lett.* **2009**, *9*, 3749−3755.
(62) Semonin, O. E.; Luther, J. M.; Choi, S.; Chen, H.-Y.; Gao, J.; Nozik, A. J.; Beard, M. C. *Science* **2011**, *334*, 1530−1533.
(63) Liu, Y.; Tolentino, J.; Gibbs, M.; Ihly, R.; Perkins, C. L.; Liu, Y.; Crawford, N.; Hemminger, J. C.; Law, M. *Nano Lett.* **2013**, *13*, 1578−1587.
(64) Sandeep, C. S. S.; ten Cate, S.; Schins, J. M.; Savenije, T. J.; Liu, Y.; Law, M.; Kinge, S.; Houtepen, A. J.; Siebbeles, L. D. A. *Nat. Commun.* **2013**, *4*, No. 2360.
(65) Ocier, C. R.; Whitham, K.; Hanrath, T.; Robinson, R. D. *J. Phys. Chem. C* **2014**, *118*, 3377−3385.
(66) Chuang, C. -H. M.; Brown, P. R.; Bulović, V.; Bawendi, M. G. *Nat. Mater.* **2014**, *13*, 796−801.
(67) Baumgardner, W. J.; Whitham, K.; Hanrath, T. *Nano Lett.* **2013**, *13*, 3225−3231.
(68) Fang, C.; van Huis, M. A.; Vanmaekelbergh, D.; Zandbergen, H. W. *ACS Nano* **2010**, *4*, 211−218.
(69) Thomas, E. L.; Kinning, D. J.; Alward, D. B.; Henkee, C. S. *Macromolecules* **1987**, *20*, 2934−2939.
(70) Bishop, K. J. M.; Wilmer, C. E.; Soh, S.; Grzybowski, B. A. *Small* **2009**, *5*, 1600−1630.
(71) Hexemer, A.; Bras, W.; Glossinger, J.; Schaible, E.; Gann, E.; Kirian, R.; MacDowell, A.; Church, M.; Rude, B.; Padmore, H. *J. Phys.: Conf. Ser.* **2010**, *247*, No. 012007.
(72) Ilavsky, J. *J. Appl. Crystallogr.* **2012**, *45*, 324−328.
(73) Yu, W. W.; Falkner, J. C.; Shih, B. S.; Colvin, V. L. *Chem. Mater.* **2004**, *16*, 3318−3322.